ISSN 0015-4628, Fluid Dynamics, 2014, Vol. 49, No. 6, pp. 748–760. © Pleiades Publishing, Ltd., 2014.
Original Russian Text © S.N. Yakovenko, 2014, published in Izvestiya Rossiiskoi Akademii Nauk, Mekhanika Zhidkosti i Gaza, 2014, Vol. 49, No. 6, pp. 54–69.

The Effects of Density Difference and Surface Tension on the Development of Rayleigh–Taylor Instability of an Interface between Fluid Media

S. N. Yakovenko

Khristianovich Institute of Theoretical and Applied Mechanics,
ul. Institutskaya 4/1, Novosibirsk, 630090 Russia
e-mail: yakovenk@itam.nsc.ru, s.yakovenko@mail.ru

Received January 30, 2014

Abstract—To describe the evolution of an interface between two immiscible media, an equation for a volume fraction function is derived, with the interface curvature effect being described by a "continuum model" of a surface tension force. A numerical study of the Rayleigh–Taylor instability problem is performed for different density ratios ρ_1/ρ_2 on the interface, including the real cases corresponding to available experimental data. At the initial stage, the instability development is independent of ρ_1/ρ_2 and consistent with the Taylor linear theory, then (for $\rho_1/\rho_2 < 5$) a spiral-like Kelvin–Helmholtz instability structure is observed. For $\rho_1/\rho_2 < 2$, the instability development pattern remains symmetric until large times when (same as for large ρ_1/ρ_2) an asymmetry appears. The surface tension and the viscosity result in the suppression of the Rayleigh–Taylor instability disturbances and secondary small-scale irregularities of the interface.

Keywords: Rayleigh–Taylor instability, interface, numerical modeling.

DOI: 10.1134/S0015462814060064

One of the most interesting and intriguing phenomena in mechanics of fluid, gas, and plasma is the Rayleigh–Taylor instability (RTI), developing on an interface between layers of a heavy (upper) and lightweight (lower) liquid media. This instability is observed from micro- to astrophysical scales, for example in the Crab nebula. The atomization of interstellar gas ejected from the galaxy plane by magnetic fields and cosmic rays may occur in accordance with the RTI scenario. Similar processes take place in supernova bursts [1, 2], in artificial and natural objects with thermonuclear synthesis, in controlled combustion reactions and fires, in Earth's mantle, oceans and atmosphere with a significant influence on the climate. One effect associated with RTI is the turbulence development and the intensification of mixing due to convective transport. At the recent international conferences on turbulent mixing, much attention was payed to the RTI effects (for example, see [3]). An example of substantial interest of the international community in this problem is the cooperation of the biggest world centers in the numerical simulation of RTI [4]. The largest known calculation of three-dimensional RTI [1] was carried out for a cubic domain with 3072^3 grid points, which required about two weeks and 65536 processors (i.e. the full power of the biggest IBM BlueGE/L supercomputer).

Most experimental and numerical studies of RTI were performed within the classical formulation for two layers of immiscible media or for a stratified medium with a step-wise or liner density profile (for example, see [5]). The evolution of RTI in conditions close to real environmental flows is still not clear understood. Recently, it was shown [6] that in the breaking of internal waves in stably stratified flows the RTI effects are also manifested, which possibly initiate the transition to turbulence. The breaking of internal waves is one of the main sources of geophysical turbulence; however, the mechanisms of the instability developing in the convective breaking of the waves are not still well studied. For a more clear understanding of specific

features of RTI, the investigations of disturbance evolution on the interface between two layers with different densities remain topical.

To describe the development of RTI, it is necessary to design adequate methods for the resolution of the interface between the regions of immiscible media. The obvious conditions here are the smallness of the calculated interface, as compared to other characteristic length scales, and the efficiency and stability of the numerical algorithm.

One widely used method for the resolution of the interface is the concept of the volume fraction of the medium (VOF) [7], defining the function f of the volume fraction, which is equal to unity in the region occupied by the denser medium and zero in the region of the less dense medium. The equation formulated for f corresponds to the motion of the volume fraction function with the fluid. To approximate advection, in [7] a special 'donor-acceptor' procedure was developed, which included the upwind or downwind schemes, depending on the surface orientation. The VOF method was used in many papers, for example, for modeling a solid-body rotation [8] and RTI. Ensuring a sharp interface, this approach results in the generation of false isolated structures, like floating fragments [8].

To reduce the errors and improve the description of the interface, different modifications of the VOF method and other approaches were proposed, for example, the MUSCLE schemes [9] with high-order interpolations. In these schemes, to control the false oscillations, appearing in the high-order methods near discontinuities, the functions-limiters are introduced for the "total-variation diminishing" (TVD). In particular, a TVD limiter in the form of a "contraction" operator, proposed in [9], gives satisfactory results both for velocity and density distributions, and for the function f. On the other hand, the interface is no longer so sharp as in the VOF method. It can have the thickness of several grid cells. Nevertheless, in this case the location of the interface can be determined by finding the points at which $f = 0.5$.

To describe the interface at small linear scales, it becomes significant to take into account the effects of surface curvature and surface tension. One of effective numerical approaches for the account of the surface tension is the 'continuum model' [10].

In the present work, we will study the evolution of RTI on the interface between immiscible fluid media with different density ratios (ρ_1/ρ_2) (characterized by the Atwood number $A = (\rho_1 - \rho_2)/(\rho_1 + \rho_2)$) using numerical methods developed in [9-12]. The calculated characteristics are compared with the linear theory [13], the experimental studies of the "water-benzene" and "water–air" interfaces [14], and the numerical results of other authors. The development of RTI is a classical problem of fluid mechanics, used in some studies [7–11, 15–21] for the verification of the interface resolution methods and the account of the surface tension effects. In particular, in [15–20] the effect of the density ratio on the evolution of RTI was detected. However, the modeling of real conditions and the comparison with experimental data were performed only in a small number of publications, and the results of the comparison (for example, in [15]) were often unsatisfactory.

1. MAIN EQUATIONS AND NUMERICAL SCHEMES

As the basic equations, we used the Navier–Stokes and continuity equations, and the equation for the volume fraction f for incompressible flow with account of surface tension [11]:

$$\frac{\partial u_i}{\partial x_i} = 0, \tag{1.1}$$

$$\frac{\partial u_i}{\partial t} + \frac{\partial u_i u_k}{\partial x_k} = -\frac{1}{\rho}\frac{\partial p}{\partial x_i} + \frac{1}{\rho}\frac{\partial}{\partial x_k}\left[\mu\left(\frac{\partial u_i}{\partial x_k} + \frac{\partial u_k}{\partial x_i}\right)\right] - g\delta_{i3} + F_i, \tag{1.2}$$

$$\rho = \rho_1 f + \rho_2(1 - f), \qquad \mu = \mu_1 f + \mu_2(1 - f),$$

$$\frac{\partial f}{\partial t} + \frac{\partial u_i f}{\partial x_i} = 0, \tag{1.3}$$

where u_i are the velocity components, x_i are the coordinates, g is the gravity force acceleration, μ is the dynamic viscosity, ρ is the density, p is the pressure, and t is time. The values ρ_1 and μ_1 correspond to the heavier fluid with $f = 1$, and the values ρ_2 and μ_2 to the light-weight fluid (gas) with $f = 0$.

For solving the main equations, as in [11, 12], we use a fairly simple procedure of simultaneous iterations of the velocity and pressure values, obtained from (1.1)–(1.2). This procedure is based on the artificial-compressibility method, with the relaxation with respect to a pseudo-time to satisfy the continuity equation. The differential equations (1.1)–(1.3) are approximated on a straggled grid to prevent the mismatch of the velocity and pressure fields: the velocity components are determined at the centers of the grid cell sides, and the scalar quantities p, f, ρ, and μ at the cell centers. For the derivatives over time and pseudo-time, we used the first-order schemes. For the terms with the molecular diffusion in (1.2) we used the central differences.

In [12], a hierarchy of five different methods of approximation of the advection terms in (1.2)–(1.3) is given, and these methods are verified with the reference to the dam-break problem. In particular, the "donor-acceptor" procedure, used in the VOF method [7], ensured a sharp interface but resulted [12] in the appearance of false structures like "floating fragments", as in [8]. The most satisfactory results with a fairly thin interface of a smooth shape were obtained using the MUSCL scheme with QUICK interpolations and TVD limiters of the contraction operator type, proposed in [9]. This scheme is used in the present study for the approximation of advection. In a more detail, the algorithms of solution of Eqs. (1.1)–(1.3) (without surface tension) are described in [12], where a good agreement of the calculations with experimental data was achieved. Following the CSF model [10, 11], the surface tension effects are introduced in the Navier–Stokes equations (1.2) in the form of the volume forces:

$$F_i = \frac{\sigma \kappa n_i}{\rho[f]}, \quad \kappa = -\frac{\partial n_m^*}{\partial x_m}, \quad n_m^* = \frac{n_m}{\sqrt{n_k n_k}}, \quad [f] = f_2 - f_1 = 1. \tag{1.4}$$

Here, σ is the surface tension coefficient, κ is the interface curvature, and n_i is the normal vector to the interface.

The most correct representation of the smoothed volume fraction function f_s assumes its smooth variation across the interface of a finite thickness (of the order of several grid cells) due to the convolution of f with the interpolation function of the core [10]. However, in the first approximation the function f_s can be taken equal to the volume fraction function, found numerically [11] (i.e. in the simplified version of the CSF model, $f = f_s$) in connection with the possible smearing of the distributions $f(x_i)$ due to the scheme viscosity. A finite-difference analog of (1.4) for two-dimensional flows with the boundaries corresponding to walls and symmetry planes is given in [11], together with the details of numerical realization of Eqs. (1.1)–(1.3) with account of the surface tension for the description of RTI of the interface between two immiscible media. In [9, 11, 21], the viscosity and surface tension effects on the development of RTI in the linear stage are considered for $\rho_1/\rho_2 = 2$, and a good agreement between the theoretical estimates and the experimental data is obtained.

2. RESULTS OF THE MODELING

For the comparison with the experimental results of [14], obtained for the verification of linear theory [13], and the calculations made using a vortex sheet method [15], at $t = 0$ a small cosine disturbance of the horizontal interface between the layers of two immiscible media was introduced:

$$y_s(x) = y_{s0}\cos(2\pi x/\lambda), \qquad y_{s0} \ll \lambda.$$

Here, $\lambda (= 2L)$ is a wave length of the imposed vertical (over the y-axis) disturbance, and L is the width of the calculation domain width in the x-coordinate (see Fig. 1, at the left, for $t = 0$). In this case, the velocity was assumed to be zero.

A similar disturbance was introduced not only in [13–15] but also in numerical studies [18–20]. In [9, 11, 16, 17, 21] a small cosine disturbance, attenuating exponentially with distance from the interface (horizontal plane), was imposed on the velocity distributions.

The initial field of the volume function takes the form: $f(x, y) = 1$ for $y > y_s$ (for the denser medium), $f(x, y) = 0.5$ at $y = y_s$ (in a thin transition zone between the media, with the thickness $\delta \ll \lambda$, the values of f vary from 0 to 1). The initial pressure distribution is hydrostatic. The left and right boundaries are assumed to be symmetry planes, and the top and bottom boundaries to be solid walls. The size of the grid sells, as in [11], was taken equal to: $\Delta x = \Delta y = L/40$. The height of the calculation domain was taken equal to $8L$ (from $y_{\min} = -4L$ to $y_{\max} = 4L$) for $\rho_1/\rho_2 < 5$ and increased to $16L$ ($y_{\min} = -12L$, $y_{\max} = 4L$) for $\rho_1/\rho_2 \geq 5$, with account of the asymmetrical development of RTI with a deep penetration of thin denser-medium jets into the less dense medium, as observed in [14, 15].

In the first series of calculations, we considered the RTI on the "water-benzene" interface at room temperature (20°C) for the following parameters: $\rho_1 = 998$ kg/m^3, $\rho_2 = 879$ kg/m^3, $\mu_1 = 1.00 \times 10^{-3}$ kg/(m s), $\mu_2 = 6.52 \times 10^{-4}$ kg/(m s), $\sigma = 0.035$ kg/s^2. The other parameters were taken as in variant 45 of the experiments [14] (different "variants" correspond to different conditions of measurements [14], and the numeration of the variants corresponds to that in [14]): $g = 305$ m/s^2, $\lambda = 0.03$ m, $y_{s0} = 0.015\lambda$, where g is the sum of the accelerations of the gravity force and the moving set-up. We note that the quantities λ and y_{so} were explicitly specified in [14]. They were found using the information presented in Figs. 12 and 16 from [14].

The Reynolds number representing the viscosity effect is defined as $\mathrm{Re} = (\lambda g)^{1/2}\lambda/\nu$ (for example, in [9] this form was used in describing the RTI with a constant viscosity $\nu = \nu_1 = \nu_2$, where $\nu_1 = \mu_1/\rho_1$ and $\nu_2 = \mu_2/\rho_2$), and the mean kinematic viscosity of two media was $\nu = (\mu_1 + \mu_2)/(\rho_1 + \rho_2)$ [17]. We can also introduce the instability parameter $\Phi = 4\pi^2\sigma/[(\rho_1 - \rho_2)g\lambda^2]$, which characterizes the surface tension effect [10, 11, 12]: for $0 < \Phi < 1$, the disturbance growth is retarded and for $\Phi \geq 1$ completely stops due to the action of the surface tension. For the above values of parameters in variant 45 of the experiment [14], the Reynolds number is fairly large $\mathrm{Re} = 1.03 \times 10^5$, and the instability parameter is small: $\Phi = 0.0422$. We may expect that the viscosity and surface tension effects will be insignificant. To check the latter effect, we performed calculations separately for $\Phi = 0$ and $\Phi = 0.0422$, which showed (see Figs. 1a, 1b, and 2) that, although the surface tension makes a slight impact on the details of RTI structures, the general instability development pattern turns out to be the same in both cases. Moreover, both the modified and simplified versions of the CFS model give identical results, particularly for a small relative value of the surface tension coefficient. Accordingly, we used the simplified model, in which $f_s = f$. We also estimated the effect of viscosity by varying the value of g by one or two orders of magnitude: the results were almost unchanged (not shown in Figs. 1, 2).

Figures 1 and 2 show the isolines $f = 0.5$, corresponding to the "water-benzene" interface, and the dependence of the hyperbolic arccosine of the mean disturbance amplitude $y_a = (y_s(x = 0) + y_s(x = L))/2$ on the normalized time $t^* = t(0.25gA/L)^{1/2}$.

The development of RTI for $t^* < 1$ agrees with linear theory [13], i.e. it follows the linear instability laws. For $1 < t^* < 2$, the secondary disturbances of the Kelvin–Helmholz instability (KHI) type develop due to the increase in the velocity shear between the counter-directed flows of two media. For $t^* > 2$, an intense vortex of the KHI breaks up, which is accompanied by a spiral swirl of the flow, the mutual penetration of the jets of two media increases, and several vortices of the KHI are formed on the interface (Fig. 1). For $t^* > 2.6$, irregularities develop gradually on the interface, which is likely associated with the large Reynolds number effects.

For small amplitudes of the initial disturbance, the value of y_a (Fig. 2) corresponds to the experimental data for $t^* \sim 0.8$. The deviation of the experimental points for $t^* \sim 0.6$ is attributable likely to the measurement errors in [14], in particular, to the limitation of the photo camera resolution at the initial instants of time for fairly small values $y_{s0} \sim 0.45$ mm. With increase in y_{s0}, the nonlinear stage of the RTI development begins at smaller t^* (Fig. 2). The instability development pattern does not change (Fig. 1) but is shifted in time. This is because the transition from the linear to nonlinear stage occurs at a certain fixed

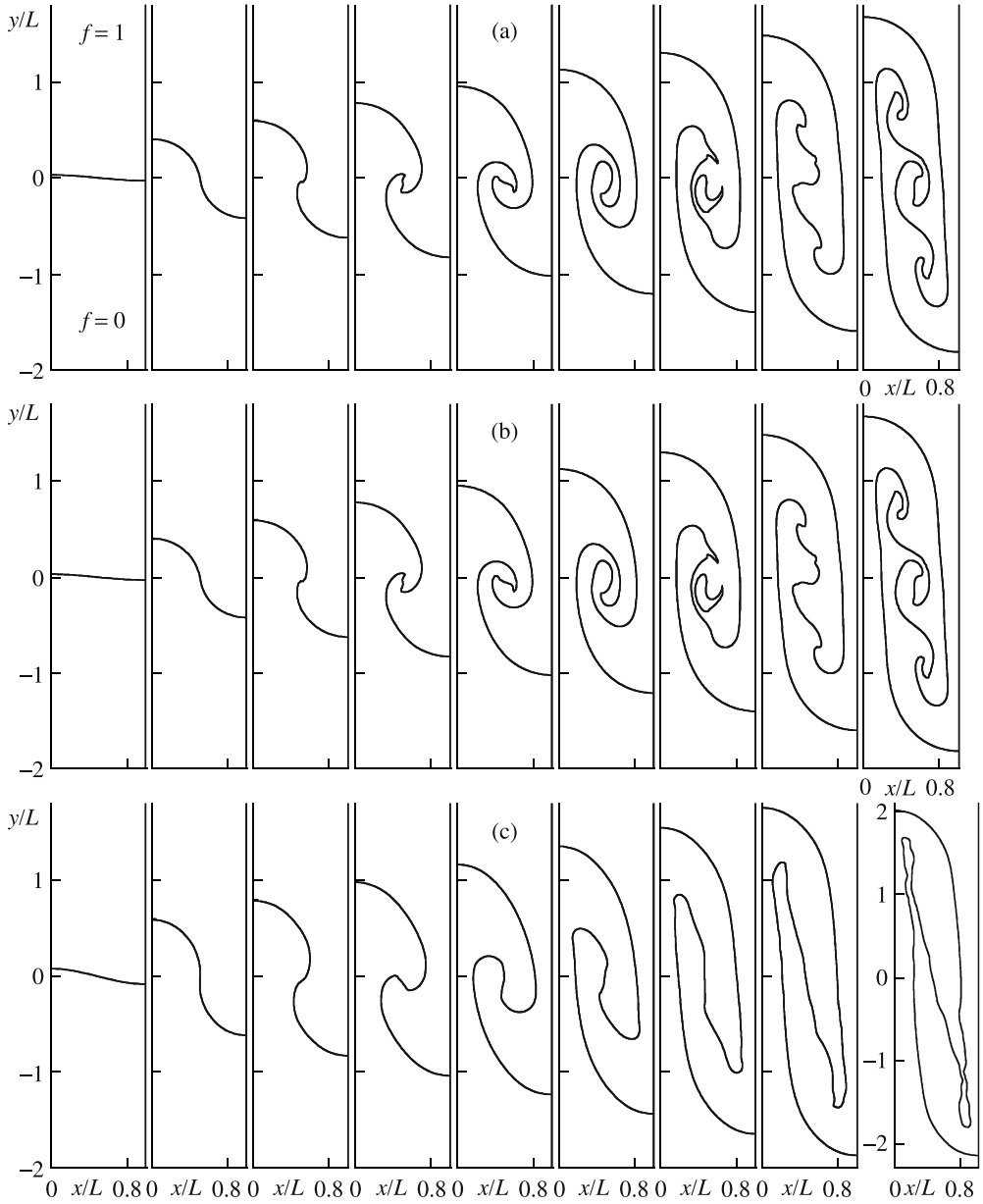

Fig. 1. Isolines of the volume fraction ($f = 0.5$) on the interface between water ($f = 1$) and benzene ($f = 0$) for $t^* = 0$, 1.1, 1.3, 1.5, 1.7, 1.9, 2.1, 2.3, and 2.5 (from left to right): (a–c) $\Phi = 0$, 0.0422, 0.333; $y_{s0}/L = 0.03$ (a, b), 0.08 (c).

interface amplitude ($y_a \sim L$, according to the data of [14, 17]), i.e. as the value y_{s0} increases, the ratio y_a/y_{s0} corresponding to this transition decreases.

The comparison with the data of [14] was performed also in [15], where a vortex sheet method was used for modeling. However, in [15] two last experimental points for $t^* \sim 0.8$ were omitted (see Fig. 2). These points where specially discussed in [14] in comparison with theory [13], and a much greater value of the stability parameter was taken ($\Phi = 1/3$) than in variant 45 of [14]. This is why the results of [15] may be insufficiently accurate and the conclusions incorrect. In particular, curve *3* in Fig. 2, corresponding to the calculations [15], lies much lower than the last two experimental points (for $t^* \sim 0.8$) and is broken too early (at $t^* \sim 1.1$), which indicates the shortage of the algorithm of inviscid calculations in [15]. For comparison with the data [15], in our calculations (Fig. 1c) we took the same parameters $\Phi = 0.333$ and y_{s0} as in [15]. The comparison of the amplitude of RTI shows the agreement of the results. A small discrepancy is associated probably with the specific features of the numerical algorithm, in particular, with the infinite

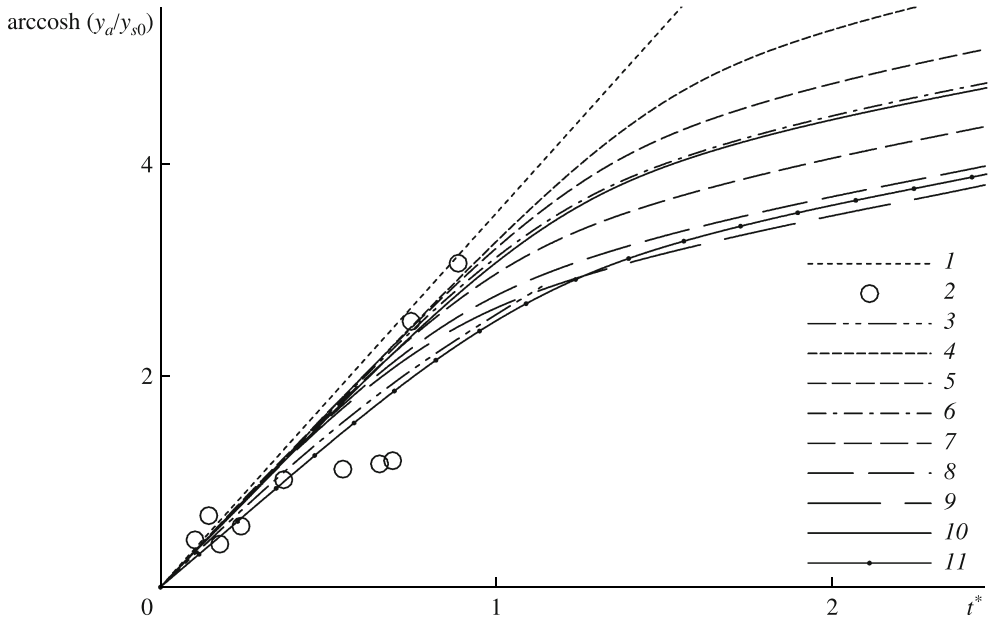

Fig. 2. Evolution of the relative amplitude of the interface: (*1*) linear theory [13]; (*2*) measurements in the "water–benzene" system [14]; (*3*) calculations using the vortex sheet method [15]; (*4–9*) calculations for $\Phi = 0$ and $ys0/L = 0.01$, 0.02, 0.03, 0.05, 0.08, and 0.10; (*10*) calculation for $\Phi = 0.0422$ and $y_{s0}/L = 0.03$; (*11*) calculation for $\Psi = 0.333$ and $y_{s0}/L = 0.08$.

Reynolds number in [15]: due to additional damping effect of the viscosity, in our calculations curve *11* in Fig. 2 lies slightly lower than curve *3*. The increased effect of surface tension also leads to damping the growth rate (see curves *8* and *11* in Fig. 2) and opposes to the spiral swirl of KHI (Fig. 1c).

In the second series of calculations, we considered RTI on the "water–air" interface, for which at a temperature of 20°C the parameters were: $\rho_1 = 998$ kg/m^3, $\rho_2 = 1.20$ kg/m^3, $\mu_1 = 1.00 \times 10^{-3}$ kg/(m s), $\mu_2 = 1.82 \times 10^{-5}$ kg/(m s), $\sigma = 0.073$ kg/s^2. The other parameters in measurement variants 2, 7, and 28, described in detail in [14], were in the ranges 193 m/s$^2 \le g \le 503$ m/s^2, 0.0102 m $\le \lambda \le 0.038$ m, $0.0295 \le y_{s0}/\lambda \le 0.0625$, which gives the values $0.004 \le \Phi \le 0.068$, $2.03 \times 10^4 \le \mathrm{Re} \le 1.62 \times 10^5$. The calculations of [15] were performed for $\Phi = y_{s0}/\lambda = 0.04$, which corresponds approximately to the middle of the intervals for Φ and y_{s0}, i.e. represents well the realizations of the measurements [14] and is close to the conditions of variant *2* (where $\Phi = 0.0335$ and $y_{s0} = 0.041\lambda$).

For comparison, in this study as the basis (Fig. 3) we took the same values ($\Phi = y_{s0}/\lambda = 0.04$ as in [15]. The acceleration is taken equal to $g = 193$ m/s^3, as in variant *2* of experiments [14], and from the definition of Φ we obtain $\lambda = 0.0193$ m (which is close to $\lambda = 0.0211$ m from variant *2*). The corresponding Reynolds number ($\mathrm{Re} = 3.65 \times 10^4$) is fairly large, and the instability parameter is fairly small, so we could expect that the viscosity and surface tension effects were small. However, the results presented below clearly illustrate the presence of both these effects.

In modeling the RTI in the "water–air" system (Figs. 3, 4), the results are well reproduced both for the linear stage and the nonlinear stage (with the saturation of the disturbance amplitude growth for large times). If the density difference on the interface is not too large, at the nonlinear stage the KHI effects are manifested, with the growth of typical mushroom-like convective structures, which is clear in Fig. 1 for $\rho_1/\rho_2 = 1.14$ and the results of [11] for $\rho_1/\rho_2 = 2$. On the other hand, for $\rho_1/\rho_2 \gg 1$ (in particular, $\rho_1/\rho_2 = 829$ in the "water–air" system) the KHI effects are absent. Instead, the fast and deep asymmetric penetration of the denser medium into the lower dense medium occurs. In this case, narrow long jets of water are formed between thick and high columns of air with smoothed upper boundaries (see Fig. 3 for $t^* > 1$), as in [14, 15].

The neglect of the surface tension, i. e. the use of the CSF model with $\sigma = 0$, for $t^* > 1$ results in the distortion of the interface for $y/L \sim 0.6$. This distortion increases with time, and at $t^* \sim 1.8$ the interface is

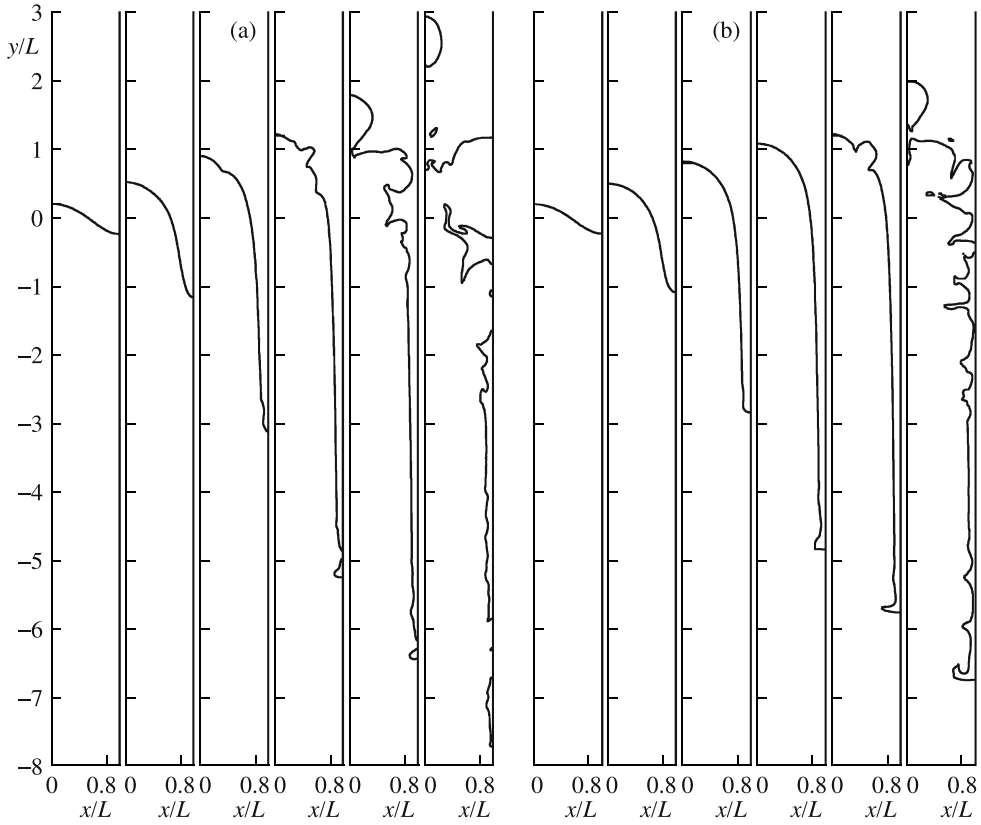

Fig. 3. Isolines of the volume fraction ($f = 0.5$) on the "water–air" interface at the instants $t^* = 0.5$, 1.0, 1.5, 1.9, 2.1, and 2.3 (from left to right): $\Phi = 0$ (a) and 0.04 (b).

fragmented near the right boundary (Fig. 3a). In the calculations with a varied parameter g (the results are not presented in the graphs), these effects are manifested earlier for larger Reynolds numbers. On the other hand, taking the surface tension into account in accordance with model (1.4) makes it possible to predict more adequately the evolution of counter-directed jets of water and air and the vertical growth of the disturbance amplitude within the scatter of the data of [14] (Figs. 3b and 4). Small-scale irregularities observed at the nonlinear stage are, apparently, unavoidable for flows with high Reynolds numbers or inviscid flows (as mentioned in [15]). However, in contrast to calculations [15], these irregularities do not lead to insoluble problems of numerical realization for time instants corresponding to the experimental data [14].

It is worth noting that the distortion of the interface at large times (Fig. 3) is not only a numerical artefact. The estimate of the disturbance wave length for the most unstable RTI mode, which grows maximally at the linear stage, gives (without surface tension) $\lambda_m = 4\pi\nu^{2/3}/(gA)^{1/3} \approx 0.00022$ m (for example, see [17]), i.e. the value of the order of the grid cell size ($\Delta x = 0.00024$ m) for the parameters considered. When the surface is taken into account, in accordance with the differentiation of the RTI growth rate (for example, see [10, 15]), the most unstable mode corresponds to $\Phi = 1/3$, from which we have $\Delta x \ll \lambda_m (\approx 0.00669 \text{ m} < L)$. It means that small disturbances, always appearing in the calculations due to the discretization and rounding errors (or random disturbances in real conditions), will gradually result in the distortion of the interface both for $\Phi = 0$ and for $\Phi > 0$, particularly at those points where the surface curvature is maximal, as is clear in Fig. 3.

The vortex sheet method [15], in which the viscosity is ignored, underestimates the RTI growth rate and is applicable only for a very short time interval (Fig. 4), since the growing irregularities of the interface do not allow to reproduce numerically the further development of the RTI disturbances. In the calculation with $\Phi = 0$ in [15], these irregularities appeared as a small break of the interface in the vicinity of the top point of the air bubble, formed as a result of the primary instability, and then resulted in the development of a

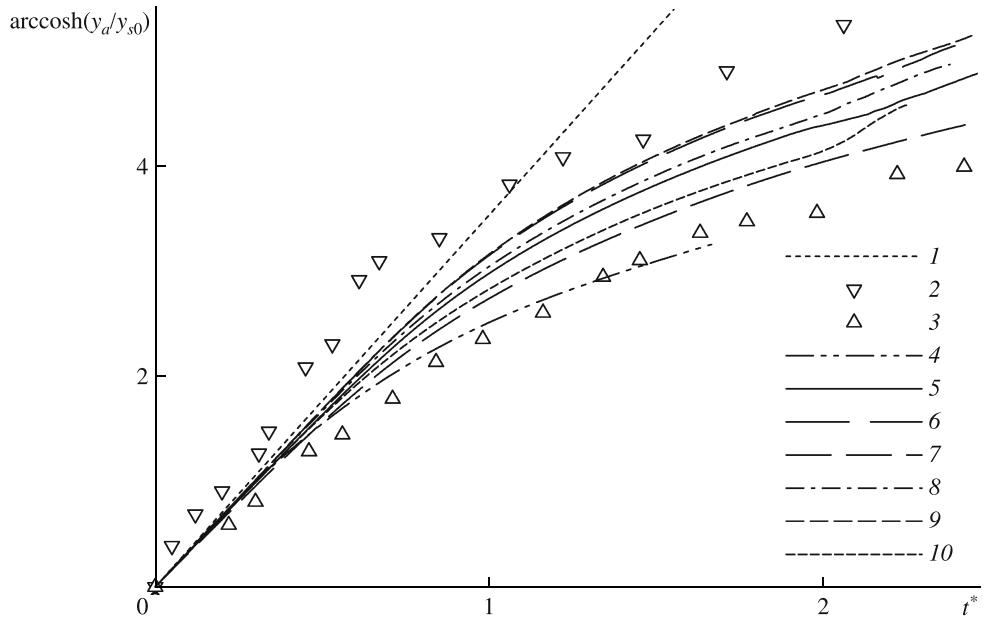

Fig. 4. Evolution of the amplitude of the "water–air" interface: theory [13] (*1*); upper and lower limits of data scatter [14] (*2*, *3*); calculations [15] (*4*); calculation for $\Phi = 0$ (corresponding to variants 2, 7, and 28 from [14]) (*5–7*); calculations for $\Phi = 0.04$ (corresponding to the same variants) (*8–10*).

secondary small-scale RTI in the bubble region and the onset of a singularity of the interface curvature. In our study, we also observed a similar distortion of the upper part of the bubble (Fig. 3a) but, in contrast to the inviscid calculations [15], it occurred much later due to the smoothing effect of viscosity at finite Reynolds numbers. On the other hand, when the surface tension was taken into account with $\Phi = 4$ in [14], the secondary instability at the upper part of the bubble was no longer observed, and the calculations could be performed for $y_a(t) < 2L$, i.e. until the amplitude of the "water–air" interface did not exceed the doubled wave length of the initial disturbance. To that time, due to the surface tension effect preventing the onset of a too large curvature, on the tip of the heavy-fluid jet a convex thicker part appeared, with a fast development of small-scale irregularities, which made impossible further calculations in [15].

In our calculations, the surface tension effect prevents the onset of the secondary instability near the top of the air column until much greater times (Fig. 3b) than in the inviscid calculations [15], due to the viscosity effect mentioned above. A similar thicker part on the tip of the water jet appears for $t^* \geq 1.4$, and for $t^* > 2$ (i.e. for $y_a(t) > 3L$) small-scale irregularities appear, which, in contrast to [15], do not result in the immediate interruption of the calculations. A similar thickening of the heavy-fluid jet occurs in real conditions on the interface with a large density difference, as follows, for example, from the experimental data of [22] for $\rho_1/\rho_2 \sim 10^3$.

The distortion of the interface generates weak oscillations of the RTI growth rate for $t^* > 2$, and the neglect of the surface tension, in addition to the enhancement and acceleration of the distortion, results in earlier oscillations of the function $y_a(t)$ (Fig. 4). A slight acceleration of the growth of $y_a(t)$ for $t^* > 2.00$ at $\Phi = 0$ and for $t^* > 2.14$ at $\Phi = 0.4$ (curves *5*, *8*, *10*) is associated with the formation of individual bubbles (over the rising air column) after the distortion and fragmentation of the interface. These bubbles rise faster than the air column, from which they appeared (Fig. 3). Nevertheless, curve *8* of the function $y_a(t)$ for $\Phi = 0$ (which lies over curve *5* for $\Phi = 0.4$ falling directly at the middle of the experimental data scatter) is still within the range of the measurement results (Fig. 4). We also plotted the calculation results corresponding to variants *7* ($g = 503$ m/s^2, $\lambda = 0.0388$ m, $y_{s0}/\lambda = 0.0295$, $\mathrm{Re} = 1.62 \times 10^5$) and *28* ($g = 410$ m/s^2, $\lambda = 0.0102$ m, $y_{s0}/\lambda = 0.0625$, $\mathrm{Re} = 2.03 \times 10^4$) from [14] with $\Phi = 0$ and $\Phi = 0.04$ (Fig. 4), which form a "fan" of calculated curves *5–10* falling in the range of scatter of the experimental data.

The variations of the Reynolds number and the instability parameter over the ranges corresponding to the

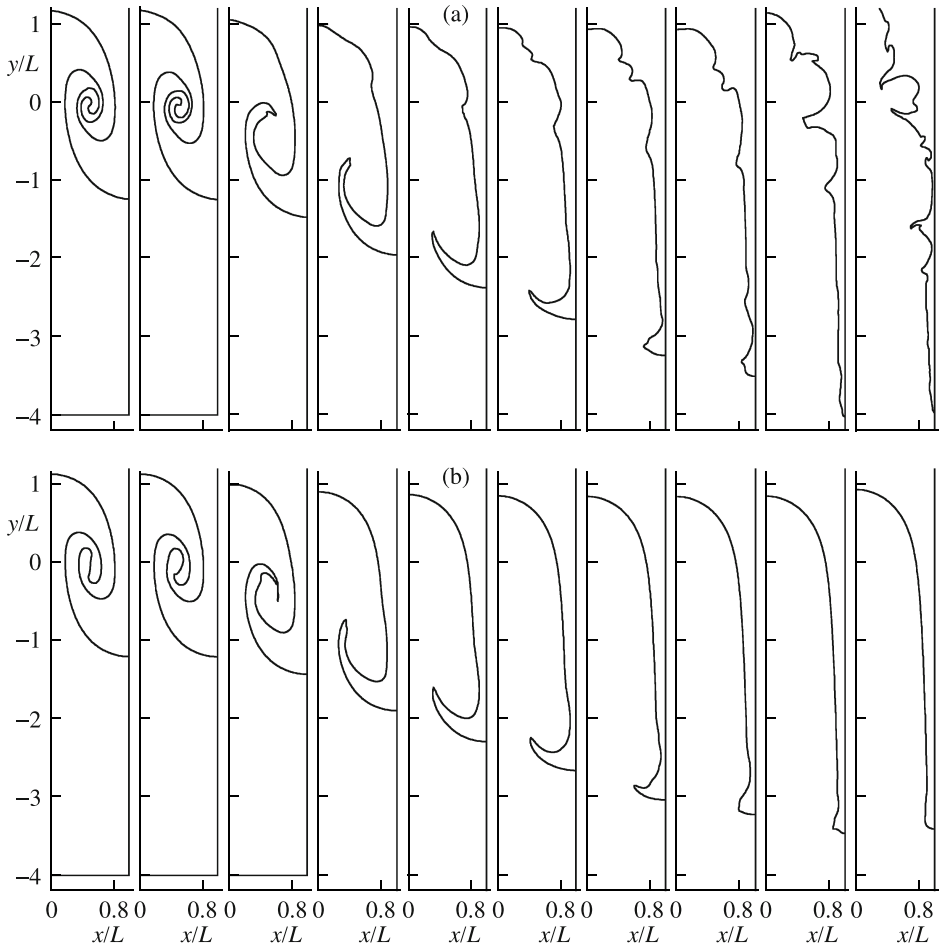

Fig. 5. Isolines of the volume fraction of water ($f = 0.5, t^* = 1.9$) on the interface between water and the less dense medium with the density ratios $\rho_1/\rho_2 = 1.01$, 1.1, 2, 5, 10, 20, 50, 100, 1000, and 10000 (from left to right): (a) $\Phi = 0$ (excluding the case $\rho_1/\rho_2 = 10000$, where $\Phi = 0.000422$); (b) $\Phi = 0.0422$.

data of [14] result in a vertical scatter of the calculation results, due to the different intensity of the damping viscosity and surface tension effects, retarding the RTI growth. As is clear from Fig. 4, an additional scatter appears in the calculations for different ratios y_{s0}/λ: larger values of the initial disturbance amplitude give an earlier deviation from the behavior, typical of the linear stage, i.e. towards the smaller values of $y_a(t)/y_{s0}$. However, at the initial instants all curves must be very close to each other and lie below the straight line corresponding to linear theory [13]. The existing scatter of the experimental data indicates a noticeable deviation from this line even for small times (Fig. 4), which is attributable to the dependence of the vertical location of the measured data on y_{s0} [14]. This parameter, varied over a wide range 0.13 mm $\le y_{s0} \le$ 8.5 mm, was minimal of the measured quantities. The inevitable errors of these measurements resulted in a noticeable variation of the initial slope of the curves obtained in different experimental conditions [14].

In the third series of calculations, we studied the RTI evolution depending on the density ratio (ρ_1/ρ_2) (Figs. 5 and 6) for fixed parameters $\rho_1 = 998$ kg/m^3, $g = 305$ m/s^2, $\lambda = 0.03$ m, $y_{s0} = 0.015\lambda$, taken as in variant 45 of [14]. The density ρ_2 was varied, and the kinematic viscosity was taken equal to that of water $(\nu = \nu_1 = \nu_2 = 1.004 \times 10^6$ m$^2/s)$. In the linear stage ($t^* < 1$), the growth of RTI occurs identically for all density ratios. For small density ratios ρ_1/ρ_2, the instability development pattern remains symmetric up to the large times (see Fig. 1). An asymmetry appears only in small details: for example, finer KHI structures are observed for the denser medium and thicker structures for the less dense medium.

As ρ_1/ρ_2 increases, for $t^* > 1$ an asymmetry in the development of RTI becomes clear from the comparison of the interface amplitude on the left and right boundaries of the calculation domain (Fig. 5). The depth

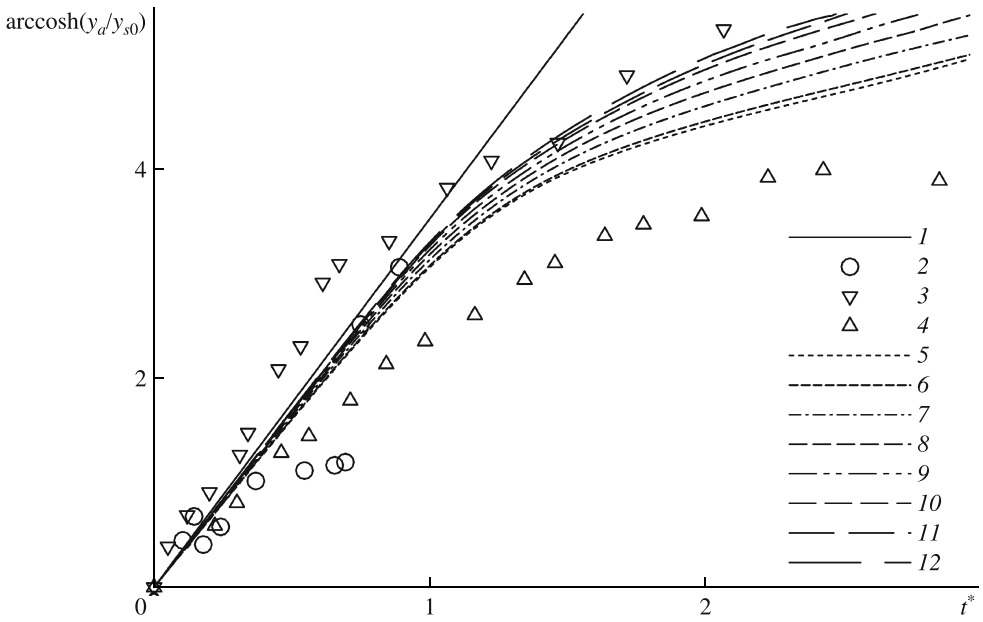

Fig. 6. The interface amplitude as a function of time and the density ratio of the media: (*1*) theory [13]; (*2*) measurements [14] for the "water–benzene" interface; (*3*, *4*) upper and lower limits of the scatter of experimental data [14] for the "water–air" interface; (*5–12*) present calculations for $\rho_1/\rho_2 = 1.1$, 2, 5, 10, 20, 50, 100, 1000 and $\Phi = 0.0422$.

of the penetration of the heavy-fluid jet is larger than the corresponding height of rise of the light fluid, and this difference increases with increase in the density ratio. The ratio of the thicknesses of the heavy-fluid jet and the light-fluid column decreases with increase in ρ_1/ρ_2. Starting from $\rho_1/\rho_2 \sim 5$, an intense vortex, resulting from the KHI effects, no more appears, and the secondary instability is manifested only as a thin heavy-fluid jet directed upward, i.e. opposite to the original jet directed downward. With increase in ρ_1/ρ_2, this small jet gradually decreases and disappears for $\rho_1/\rho_2 \sim 50$, when only a thicker part remains on the tip of the main heavy-fluid jet falling down. The latter in turn disappears for $\rho_1/\rho_2 > 10^3$ (apparently, up to the case of flow into vacuum). We note that when the surface tension is neglected (Fig. 5a), for $\rho_1/\rho_2 > 2$ and $t^* > 1.9$ a distortion of the interface becomes noticeable. This distortion increases with increase in the density ratio. For $\rho_1/\rho_2 = 10^4$, $\Phi = 0$, and $t^* > 1.7$, this results in the intense fragmentation of the interface, i.e. in the atomization of the water and air jets into droplets and bubbles (these results are not presented here). The introduction of a fairly small surface tension (see Fig. 5a for $\rho_1/\rho_2 = 10^4$ and $\Phi = 4.22 \times 10^{-4}$) retards the distortion and fragmentation. Taking the surface tension ($\sigma = 0.035$ kg/s^2, as in variant 45 from [14], which corresponds to $\Phi = 0.0422$) into account eliminates the distortion of the interface at least up to $t^* \sim 2$ (Fig. 5b).

With increase in the density ratio or the Atwood number, the amplitude of the interface as a function of the normalized time (Fig. 6) shows the trend of growth. The main differences in the amplitudes are observed on the range $2 < \rho_1/\rho_2 < 100$, whereas for $1.1 < \rho_1/\rho_2 < 2.0$ and $10^2 < \rho_1/\rho_2 < 10^3$ the differences reduce, and the curves for $\rho_1/\rho_2 = 1.01$ and 1.1 almost coincide, as for the cases with $\rho_1/\rho_2 = 10^3$ and 10^4. We note that the flow pattern shown in Fig. 1 for $\rho_1/\rho_2 = 1/14$ remains almost unchanged for $\rho_1/\rho_2 = 1.01$ and 1.1 (only the flow symmetry becomes more pronounced, as the density ratio decreases to unity). In fact, the behavior of the "water–benzene" interface may serve as an analog of the RTI development in a single-phase stratified medium at large Reynolds (and/or Prandtle/Schimdt) numbers, when the effects of molecular diffusion are insignificant, as compared with the convective transport.

It is also interesting to compare our results with the previous studies. In [17, 19], the RTI was calculated for three values of the density ratio: 3, 20, and 40. The authors observed the enhancement of asymmetry of the RTI structures and a deeper penetration of the heavy-fluid jet with increase in ρ_1/ρ_2, as in our study. In [17–19], it was noted that the KHI vortices exist on the interface of the counter-directed jets only when

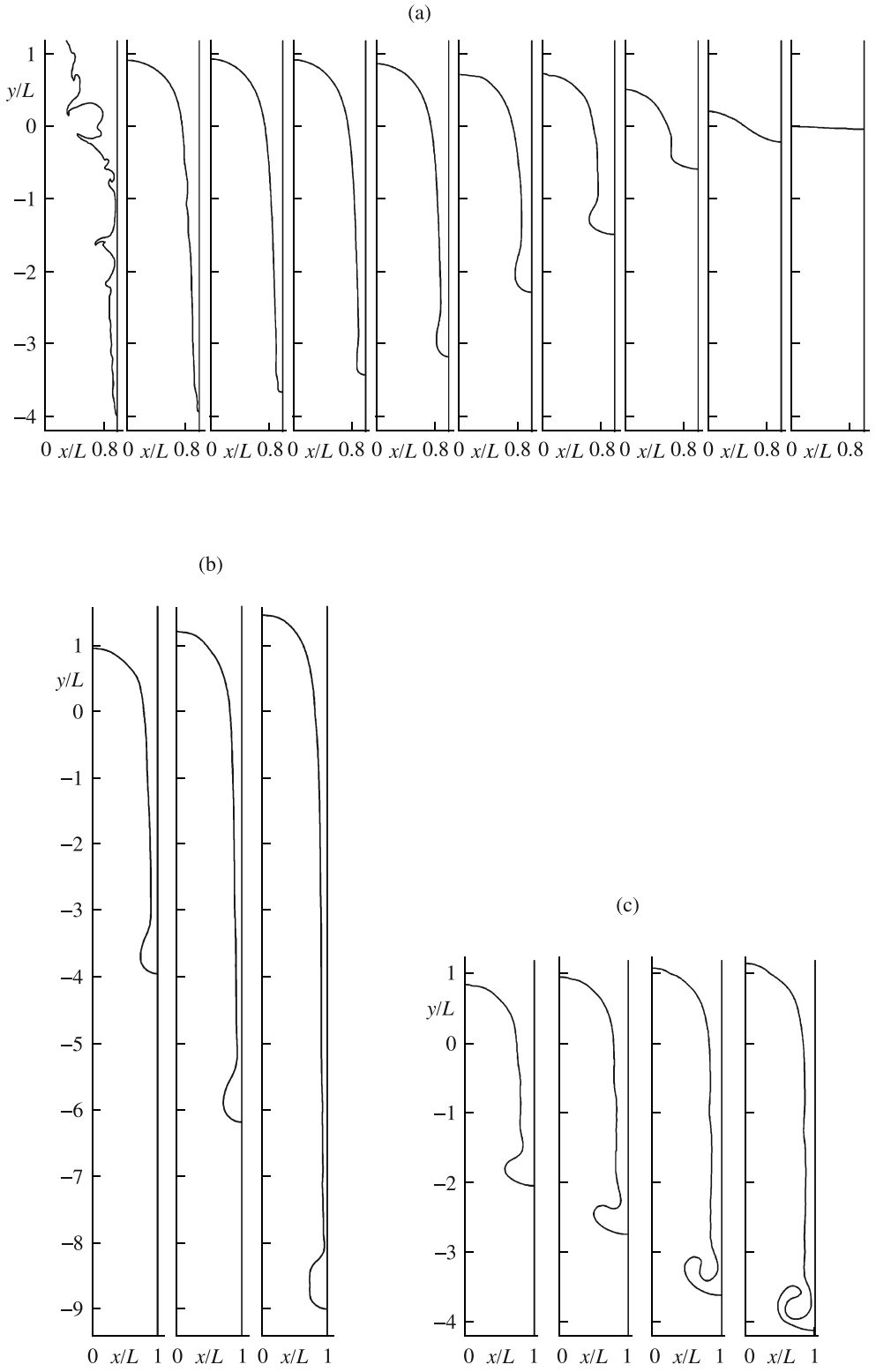

Fig. 7. Isolines of the volume fraction of water ($f = 0.5$) for $\rho_1/\rho_2 = 10000$: (a) $\Phi/\Phi_0 = 0.01$, 0.1, 0.5, 1, 2, 5, 10, 15, 20, and 25 (from left to right), $t^* = 1.9$; (b) $\Phi/\Phi_0 = 5$, $t^* = 2.3$, 2.7, 3.1; (c) $\Phi/\Phi_0 = 10$, $t^* = 2.1$, 2.3, 2.5, and 2.6.

$\rho_1/\rho_2 \le 4$ (this agrees with our conclusion of the elimination of this effect starting from $\rho_1/\rho_2 \sim 5$). In [18], the RTI was modeled using vortex methods with neglect of viscosity and surface tension effects for the ratios ρ_1/ρ_2 from unity (Atwood number A = 0) to infinity (RTI on the interface between a fluid and vacuum with A = 1). It was shown that for $\rho_1/\rho_2 = 3$, after the appearance of one KHI vortex, later the second vortex may be formed, which agrees with our results in Fig. 1 for $t^* > 2.2$. However, in the calculations of [18] for A = 1, on the tip of a long heavy-fluid jet a noticeable thick part appears, which retains with a decrease in the grid cell size. In our studies, a similar structure is observed for $\rho_1/\rho_2 = 10^3$ but disappears with the further increase in ρ_1/ρ_2 to 10^4 (see Fig. 5). With account of the fact that, in the "exact" solution the tip of the jet flowing into vacuum is sharp [20, it should be noted that, as the density ratio tends to infinity and the Atwood number tends to unity, our calculations seem to be more adequate than [18].

In the fourth series of the calculations, we studied the surface tension effect for $0.01 \le \Phi_0 \le \Phi \le 25\Phi_0$ (here, $\Phi_0 = 0.0422$). The other parameters were as in the third series, but with a fixed density ratio $\rho_1/\rho_2 = 10^4$ (Fig. 7). This case is interesting because for $\Phi = 0$ the distortion and fragmentation of the interface occur most early and in the most intense manner, and for $\Phi \ge 0.01\Phi_0$ not only this distortion is retarded but also the shape of the tip of the heavy-fluid jet changes (see Fig. 5). Indeed, when Φ increases to $0.1\Phi_0$ no distortion of the interface is observed for $t^* \sim 2$ (Fig. 7a), and the transition from the sharp tip to its thickening begins for $\Phi \sim 0.5\Phi_0$ and finishes when $\Phi \sim 5\Phi_0$. In addition, the retardation of the RTI growth occurs with increase in the surface tension, and for $\Phi = 25\Phi_0 = 1.055$ the disturbances can be even damped, which agrees with the results of modeling for $\rho_1/\rho_2 = 2$ [11, 12]. It is worth to mention the effects of thickening of the jet tip with time (see Fig. 7b for $\Phi = 5\Phi_0$) and returning to the formation of a spiral swirl of the KHI vortex for $5\Phi_0 < \Phi < 20\Phi_0$ (see Fig. 7c for $\Phi = 10\Phi_0$), similar to that occurring for small density ratios (Figs. 1 and 5). When the surface tension is large, which results in a strong retardation and slower development of the RTI, as compared to small Φ, the heavy-fluid jet becomes thicker and turns around, which illustrates the development of the KHI. We note that, with increase in the viscosity effects, as mentioned in [23] for the case A = 1, i.e. when the RTI develops on the interface between a fluid and vacuum, the thickening of the heavy-fluid jet and a decrease in its velocity are also observed. However, in [23] no KHI vortices were detected with increase in the viscosity effect.

Summary. The evolution of an interface between two immiscible media is studied by solving numerically the Navier–Stokes equations and the equation for the volume fraction function, using a continuum model for surface tension. The study of the Rayleigh–Taylor instability shows the initial exponential growth of the disturbance amplitude, which corresponds to the linear instability stage with a constant growth rate. For real media (water-benzene, water–air), a good agreement with theoretical [13] and experimental data [14] is obtained for both linear and non-linear stages. For the "water–benzene" system, the interface behavior may be regarded as an analog of the development of Rayleigh–Taylor instability in a stratified medium.

At the initial stage, the instability development is independent of the density ratio on the interface (ρ_1/ρ_2). If this ratio is not too large ($\rho_1/\rho_2 < 5$), at the non-linear stage, due to the enhancement of velocity shear between counter-directed flows of the media, the effects of the Kelvin–Helmholz instability are observed, which result in the formation of characteristic mushroom convective structures with a spiral swirl of the flow. For large density ratios (for example in the "water–air" case), thin jets of the denser fluid penetrate into the less dense medium forming high and thick columns rising upward. For $\rho_1/\rho_2 < 2$, the instability pattern remains symmetric up to large times, when (same as with increase in ρ_1/ρ_2) an asymmetry increases. The surface tension results in the decrease in the growth rate, i.e. damping the instability, prevents the distortion and fragmentation of the interface and prompts the thickening of the tip of the heavy-fluid jet and returning to mushroom structures at $\rho_1/\rho_2 \sim 10^4$.

Our results in simulating the evolution of Rayleigh–Taylor instability and studying the effects of the density ratio and the instability parameter confirm and refine the results of previous investigations.

The work received financial support from RFBR (Nos. 12-01-00050-a and 13-05-00006-a).

REFERENCES

1. W.H. Cabot and A.W. Cook, "Reynolds Number Effects on Rayleigh–Taylor Instability with Possible Implications for Type-Ia Supernovae," Nature Phys. **2**, 562–568 (2006).
2. N.J. Hammer, H.-Th. Janka, and E. Müller, "Three-Dimensional Simulations of Mixing Instabilities in Supernova Explosions," Astrophys. J. **714**, 1371–1385 (2010).
3. S.I. Abarzhi, "Review of Theoretical Modelling Approaches of Rayleigh–Taylor Instabilities and Turbulent Mixing," Phil. Trans. R. Soc. A. **368**, 1809–1828 (2010).
4. G. Dimonte, D.L. Youngs, A. Dimits, et al., "A Comparative Study of the Turbulent Rayleigh–Taylor Instability Using High-Resolution Three-Dimensional Numerical Simulations: The Alpha-Group Collaboration," Phys. Fluids **16**, 1668–1693 (2004).
5. S.I. Voropaev, Y.D. Afanasyev, and G.J.F. van Heijst, "Experiments on the Evolution of Gravitational Instability on an Overturned, Initially Stably Stratified Fluid," Phys. Fluids A. **5**, 2461–2466 (1993).
6. S.N. Yakovenko, T.G. Thomas, and I.P. Castro, "A Turbulent Patch Arising from a Breaking Internal Wave," J. Fluid Mech. **677**, 103–133 (2011).
7. C.W. Hirt and B.D. Nichols, "Volume of Fluid (VOF) Method for the Dynamics of Free Boundaries," J. Comput. Phys. **39**, 201–225 (1981).
8. M. Rudman, "Volume-Tracking Method for Interfacial Flow Calculations," Int. J. Numer. Meth. Fluids **24**, 671–691 (1997).
9. F.J. Kelecy and R.H. Pletcher, "The Development of a Free Surface Capturing Approach for Multidimensional Free Surface Flows in Closed Containers," J. Comput. Phys. **138**, 939–980 (1997).
10. J.U. Brackbill, D.B. Kothe, and C. Zemach, "A Continuum Method for Modeling Surface Tension," J. Comput. Phys. **100**, 335–354 (1992).
11. S.N. Yakovenko and K.S. Chan, "Application of a Continuum Model for the Surface Tension Force to the Rayleigh–Taylor Instability Problem," Thermophysics and Aeromechanics **18** (3), 449–461 (2011).
12. S.N. Yakovenko and K.S. Chan, "Application of Volume-Fraction Fluxes in a Two-Fluid Flow," Thermophysics and Aeromechanics **15** (2), 449–461 (2008).
13. G.I. Taylor, "The Instability of Liquid Surfaces When Accelerated in a Direction Perpendicular to Their Planes. I," Proc. R. Soc. Lond. A. **201**, 192–196 (1950).
14. D.J. Lewis, "The Instability of Liquid Surfaces When Accelerated in a Direction Perpendicular to Their Planes. II," Proc. R. Soc. Lond. A. **202**, 81–96 (1950).
15. D.I. Pullin, "Numerical Studies of Surface-Tension Effects in Nonlinear Kelvin–Helmholtz and Rayleigh–Taylor Instability," J. Fluid Mech. **119**, 507–532 (1982).
16. B.J. Daly, "Numerical Study of Two-Fluid Rayleigh–Taylor Instability," Phys. Fluids **10**, 297–307 (1967).
17. D.L. Youngs, "Numerical Simulation of Turbulent Mixing by Rayleigh–Taylor Instability," Physica D **12**, 32–44 (1984).
18. G. Tryggvason, "Numerical Simulations of the Rayleigh–Taylor Instability," J. Comput. Phys. **75**, 253–282 (1988).
19. D.L. Youngs, "Modelling Turbulent Mixing by Rayleigh–Taylor Instability," Physica D **37**, 270–287 (1989).
20. G.R. Baker, D.I. Meiron, and S.A. Orszag, "Vortex Simulations of the Rayleigh–Taylor Instability," Phys. Fluids **23**, 1485–1490 (1980).
21. B.J. Daly, "Numerical Study of the Effect of Surface Tension on Interface Instability," Phys. Fluids **12**, 1340–1354 (1969).
22. H.W. Emmons, C.T. Chang, and B.C. Watson, "Taylor Instability of Finite Surface Waves," J. Fluid Mech. **7**, 177–193 (1960).
23. F.H. Harlow and J.E. Welch, "Numerical Study of Large-Amplitude Free-Surface Motions," Phys. Fluids **9**, 842–851 (1966).